ARAI Journal of Mobility Technology
Volume 2 • Issue 2 • April–June, 2022, pp. 183-191
https://doi.org/10.37285/ajmt.1.2.3

Research Paper

Effects of Vortex Generators on Aerodynamic Drag Force in the Hatchback Type Car

Sanjay D. Patil, Vikas T. Mujmule, Ajay P. Mahale, Suhas A. Jagtap and Ganesh S. Patil

Department of Automobile Engineering, Government College of Engineering and Research, Avasari, Pune – Maharashtra.

ABSTRACT

Aerodynamic drag force is one of the main obstacles on moving a vehicle. This force significantly reduces a vehicle's speed and, as a result, its fuel efficiency. In today's scenario, fuel efficiency is a prime concern in vehicle design, so a reduction in aerodynamic drag force is highly important. Road vehicles are designed to pass through surrounding air and displace it as efficiently as possible. Due to the rear shape of a car, airflow suddenly separates from the vehicle at a point near the rear windscreen. This flow separation at the rear end of the car is responsible for the drag force, which is the main opposition to the vehicle's forward motion. This drag force is proportional to the square of the velocity of the car and, as a result, increases significantly after certain speeds. To reduce the drag force, the flow separation at the rear end needs to be avoided. In hatch-back type cars, to avoid this separation, a vortex generator (VG) can be used. VG creates the vortex at the rear end of the car, which delays the flow separation and, ultimately, drag is reduced significantly. In this work, the effect of a VG on the pressure distribution, velocity destitution and aerodynamic drag on the hatchback type car, is studied by the numerical simulation. The numerical simulations are carried out using the ANSYS FLUENT® software. The simulation setup is validated with wind tunnel test results.

KEYWORDS: Drag force; Vortex generator (VG); Aerodynamics forces; Flow separation; Velocity distribution; Pressure distribution; CFD.

Introduction

Aerodynamics is a branch of fluid dynamics that studies interactions between the air and solid bodies moving through it. The aerodynamic forces exerted on a vehicle by the air due to the relative motion of the air and the vehicle when it goes forward. This causes the resistance to vehicle's moment [1-2]. The motion of air around the vehicle is called a "flow field," which is an analysis by using various properties like velocity, pressure, density, and temperature. These properties are a function of position and time and can be calculated by using equations for the conservation of mass, momentum, and energy [3].

When a vehicle is moving, lift and drag are the two primary aerodynamic forces acting on the vehicle. The lift force is acting in the vertical direction on the vehicle body. As the effect of lift force is produced, up-thrust or down-thrust depends upon the shape of the vehicle. Up-thrust is undesirable as it reduces the tyres' ground grips, whereas down-trust enhances the tyre's road-holding [4-6]. The lift force is represented by,

$$F_L = \frac{1}{2} \rho V^2 C_L A \quad \text{.....(1)}$$

Where,

F_L= Lift force

C_L = Lift coefficient

A= Frontal area of the vehicle

V= Wind velocity

ρ = Air density

The lift coefficient C_L is a dimensionless quantity that is a measure of the difference in pressure created above and below of vehicle body, it is also used to compare the different vehicle shapes [5, 8].

From an energy-saving point of view, the aerodynamic drag force receives special attention [1-2]. The drag force acts in the opposite direction of car movement. Due to constraints created by boot space, rear windscreen, size of car, regulations, etc., cars end up being somewhat obliquely and boxy shaped. Such a shape is responsible for creating the low pressure zone behind a car in a forward motion [5]. This low pressure zone is called the "wake region" [6, 9]. During the airflow over the surface of the vehicle, in the wake region, there are some points when the change in velocity comes to stall and the air starts flowing in the reverse direction. This phenomenon is called "separation" of the flow field, which is undesirable in vehicle motion [7-8]. Ultimately, this airflow separation pulls the car from behind and opposes the forward motion of the car. This is called the "drag force." To avoid this flow separation, the transitions of the airflows from the roof to the rear window need to be smoother [7-9].

The drag force is represented by,

$$F_D = \frac{1}{2} \rho V^2 C_D A \quad \text{.....(2)}$$

F_D = Lift force

C_D = Lift Coefficient

The drag performance of vehicles is characterized by the drag coefficient (C_D) This non-dimensional coefficient allows the drag performance between different vehicles and different setups of the same vehicle to be compared directly [5, 8].

Various kinds of literature are available in the public domain on active and passive systems to minimise the drag force. In case of the active system, jets are used to create vortices, while on passive systems, a modified shape is used to reduce the wake region. The studies by Abdellah Ait Moussa et al. [13] worked on the reduction of aerodynamic drag in generic trucks using optimised geometry of rear cabin bumps. Damjanovic et al. [14] investigated the use of a spoiler to reduce race car aerodynamic drag. Computational analysis of flow separation to reduce the drag force vehicle is performed by Rouméas et al. [15]. Wang et al. [16] studied the active system for drag reduction, even with wheel-vehicle interaction drag force can be reduced. A Steady Jet Flow (SJF) system is reduced the pressure difference at the rear end, this system was used in works by Pastoor et al. [17] for drag reduction. C.H. Bruneau et al. [19] used a combination of jet actuation and a porous top layer on the Ahmed body and presented numerical results showing a remarkable drag reduction of around 31%. Salati et al. [20] examined VG in a truck model with both numerical models and wind tunnel tests and concluded the advantageous effects, besides drag and overturning moment reduction. Lee et al. [21] stated that the spoiler can reduce the vehicle's drag by 3.1%. Zhigang Yang [2] worked on the aerodynamics of pick-up trucks and described the geometrical aspects to reduce drag force. Xin-kai Li et al. [23] examined the offset between two delta-shaped winglets and concluded the maximum drag reduction was achieved at a 5 offset distance/VG height ratio. To the author's best knowledge, less exposure has been observed in the study of the effects of various numbers of VG on the pressure contours, velocity vector, and aerodynamic drag force in the case of a hatchback type car.

This paper is structured as follows. The finite volume numerical simulations are performed on ANSYS FLUENT software. The numerical simulation setup is validated with a wind tunnel test in Section 2. A similar set-up has been used in section 3 to analyse the effect of VGs on the aerodynamic characteristics of a hatchback car, namely, velocity destitution, pressure distribution, velocity vectors, and drag force. First, a car model without VGs is considered the baseline configuration, and using numerical simulation, the aerodynamic characteristics of the baseline model are evaluated. Second, on the same setup, one to five number of VGs are attached at the rear end of the car and evaluate aerodynamic characteristics. Furthermore, these aerodynamic characteristics are compared with each other and with the baseline configuration.

Experimental Validation of Simulation Setup

Vortex Generator

In various car models, VG is used to reduce the drag force. The rear end of hatchback cars is somewhat obliquely and boxy. As discussed in section 1 flow separation takes place at the rear end of the car and air starts moving in the reverse direction, which causes the drag force as shown in figure 1 [8, 21]. A VG is one of the solutions to this problem [17,21]. A VG is an aerodynamic surface made up of a small vane or bump that is attached to the back of the car because of its shape and position, which creates a vortex [20].VG controls the boundary layer transition by creating a vortex at the rear end, which delays the flow separation and, ultimately, drag is reduced significantly [19, 21, 22].

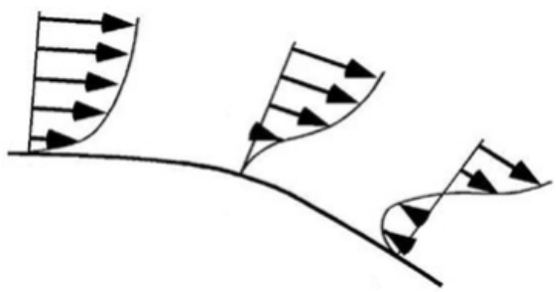

Fig. 1. Flow of air at rear end of car.

Experimental Setup on Wind tunnel test

The validation of the numerical simulation setup is to be done by using the wind tunnel test ring. The airfoil model, having a chord length of C=100 mm and a length of L= 300 mm, is placed in the wind tunnel at an angle of attack of α=50 with the free stream direction. The upstream velocity V= 15m/s and the density ρ is 1.2kg/m3. The air velocity is assumed to be steady state, inviscid, and uniform. A piezometer is used to measure the pressure difference ΔP along the length of the airfoil model. The experimental setup is shown in figure 2.

Fig. 2. Wind tunnel experimental setup.

The elemental pressure force per unit span of airfoil is can be expressed as,

$$df = \Delta P \, dl, \quad \text{.....(3)}$$

Due to airfoil model angle of attack this element pressure is divided into two component, and they are calculated by,

$$df_x = \Delta P \, dy \quad \text{.....(4)}$$

$$df_y = \Delta P \, dx \quad \text{.....(5)}$$

Therefore, total force in X and Y direction is can be evaluated by integrating the element force along the Y and X direction respectively. This is to be done by measuring the pressure using piezometer along curtain interval in the X and Y direction of airfoil model so,

$$F_x = \int \Delta P \, dy \quad \text{.....(6)}$$

$$F_y = \int \Delta P \, dx \quad \text{.....(7)}$$

Dynamic pressure on airfoil model is obtained by,

$$F = \frac{1}{2} \rho V^2 C \quad \text{.....(8)}$$

Where C is force coefficient which is have two component in X and Y direction which are,

$$C_x = \frac{Fx}{(\frac{1}{2}\rho V^2)} = \frac{\int \Delta P \, dy}{(\frac{1}{2}\rho V^2)} \quad \text{.....(9)}$$

$$C_y = \frac{Fy}{\frac{1}{2}\rho V^2} = \frac{\int \Delta P \, dx}{\frac{1}{2}\rho V^2} \quad \text{.....(10)}$$

For airfoil angle of attack $\alpha=5^0$ and piezometer angle of inclination $\theta=0^0$ the C_D and C_L are calculated by,

$$C_D = C_y \sin\theta + C_x \cos\alpha \quad \text{.....(11)}$$

$$C_L = C_y \cos\alpha - C_x \sin\theta \quad \text{.....(12)}$$

Numerical Simulation setup on CFD software

To validate the numerical simulation setup, all parameter values like velocity, the density of air, size of airfoil model, etc. are taken as the same as used in the wind tunnel experimental test in section 2.2. The airfoil 3D model is created in the SolidWork software and import into the ANSYS software for further analysis. The necessary boundary conditions like inlet velocity, outlet velocity, and wall movements are applied, and the model is mesh with an element size of 1.5. Figure 3 (a) and (b) show the velocity distribution and streamline flow around an airfoil. The C_D and C_L are obtained from simulation and compared with wind tunnel test results in Table 1.

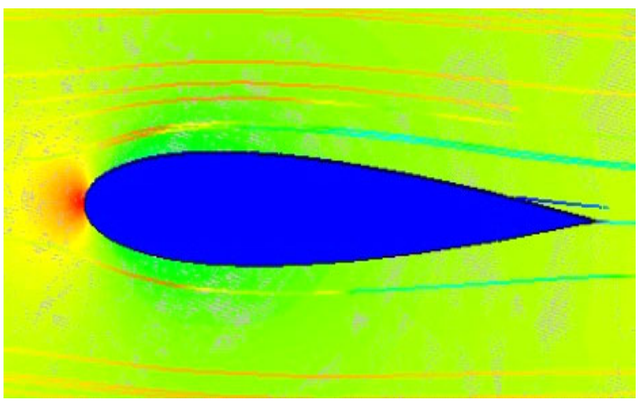

Fig. 3 (a) Velocity distribution around airfoil.

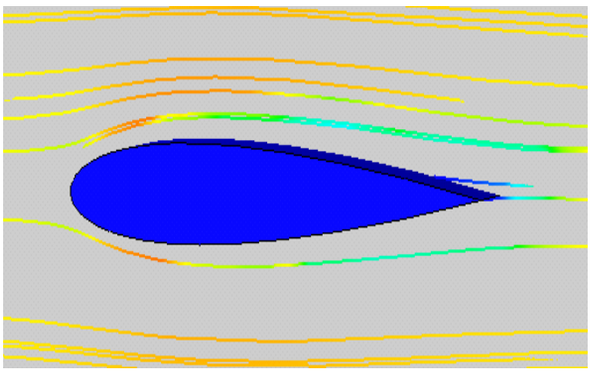

Fig. 3 (b). Velo. streamline around airfoil.

TABLE 1

Experimental and simulation results comparison

Sr. No.	Parameter	Wind tunnel experimental	Numerical Simulation	Percentage Error
1	Drag Coefficient (C_D)	0.213	0.197	9.2%
2	Lift Coefficient (C_L)	0.197	0.174	8.8%

It has been observed that the absolute error between the wind tunnel experimental test and the CFD simulation of C_D and C_L is less than 10% and they are considerably closer to each other. Hence, the above-mentioned simulation setup is considered in the present work for further study of the car model with VG and without VG.

Numerical Simulation

The hatchback car model shown in Figure 4 was selected for the study. The 3D geometrical model of the car is created in the SolidWork software and has an overall length of 3765mm, an overall height of 1500mm, and an overall width of 1690mm. As per the many kinds of literature, the optimum height of the VG is defined as being almost equal to the boundary layer thickness [5]. The most favourable size of VG is found to be 25.45 mm X 10mm of a bump-shaped piece with a rear slope angle of 25°. Figure 5 shows the dimension of VG [23,24]. The location of vortex generators is selected at a point immediately upstream of the flow separation point and a point at a distance of 100 mm from the facade of the roof end.

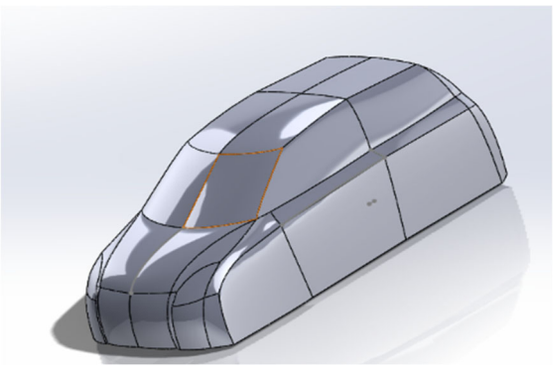

Fig. 4. Hatchback car base model.

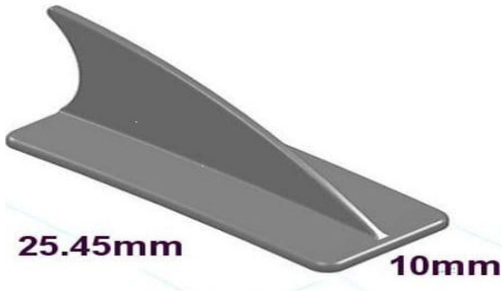

Fig. 5. Dimensions of Vortex generator.

A further computational analysis is carried out in the ANSYS FLUENT software. The car model is imported into ANSYS software. For the computational simulation, it has been assumed that the airflow is a steady-state with constant velocity at the inlet, constant pressure outlet, no-slip wall boundary conditions at the car's body, and inviscid flow wall boundary conditions at the car's surface, roof, and sidewall. The enclosure size is based on literature [21], and dimensions in X, Y, and Z directions are 6L X 2L X 2L m, respectively. The necessary boundary conduction like inlet velocity, outlet velocity, and wall movement is applied in simulation. The model is discretized with triangular elements of size 1.5. The other simulation parameters are given in table 2, and the ANSYS simulation setup is shown in figure 6.

TABLE 2

Simulation Parameters.

Sr. No	Parameter	Boundary conditions	Parameter Values
1	Velocity inlet	Magnitude measured normal to boundary	60 km/hr
2	Pressure outlet	Gauge pressure magnitude	0 Pa
		Gauge pressure direction	Normal to boundary
		Turbulence specification method	Intensity & viscosity
		Backflow turbulence intensity	10%
3	Fluid properties	Fluid type	Air
		Density (ρ)	1.175 (kg/m3)
		Kinematic viscosity (V)	1.7894 × 10–5 (kg/(m s))

To analyse the effect of VG on drag force, the first simulation (simulation 1) is performed without VG by taking the above-said parameter. During the simulation process, drag force, lift force, drag coefficient, and lift coefficient were tracked. Simulation 2 is carried out by taking the 1 number of VG mounted at the centre of the roof. The simulation parameters for simulation 2 and further simulations are kept the same as in simulation number 1. Similarly, simulations 3 to 6 are performed by taking the 2 to 5 number of VGs, respectively. For all simulations, the above-mentioned parameter values are obtained. The pressure distribution, velocity distribution, and velocity vector of all 6 simulations are plotted to analyse the flow separation. A detailed comparison of CFD results is discussed in the following section.

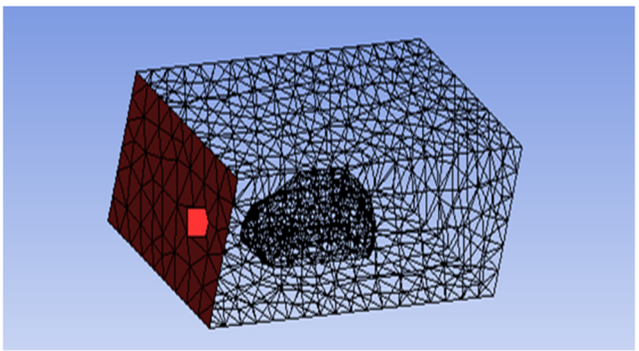

Fig. 6. ANSYS simulation setup.

Result and Discussion

All the simulations mentioned in the previous section are performed and their results, like pressure distribution, velocity distribution, velocity streamline, and value of drag force, are obtained and discussed in detail in the following subsections.

Pressure Distribution

The pressure distribution around the car model for all simulations is as expected. The high-pressure zone is depicted in red in Figures 7(a-f), and the low-pressure zone is depicted in blue.

It was observed that the pressure distribution in different areas behaves differently because of the way air particles interact with a certain portion of the car. At the front of the car, there is a direct collision of air partials, so for all simulations at the front, there is a high-pressure zone. On the other hand, at the rear end, the pressure is considerably lower. As discussed earlier, the low-pressure zone at the rear end is the main factor in creating the drag force. Figure 7 (a) shows that the low-pressure zone blue spots are more prevalent at the rear end of Simulation 1 (without VG) than in the other figures. While, in figures 7 (e) and (f) (simulations 5, and 6), low-pressure zones, blue spots are observed on the roof of the car. Low-pressure zone spots in figures 7(b) and (c) (Simulations 2 and 3) are comparable to fewer in other figures. As the number of VG increases, as in figures 7 (e) and (f) (simulations 5 and 6), low-pressure zones are observed at the roof of the car, which increases drag force at the roof of the car.

Velocity Distribution

Figure 8 (a to l) depicts the velocity distribution and velocity vectors of all simulations at a symmetry plan.

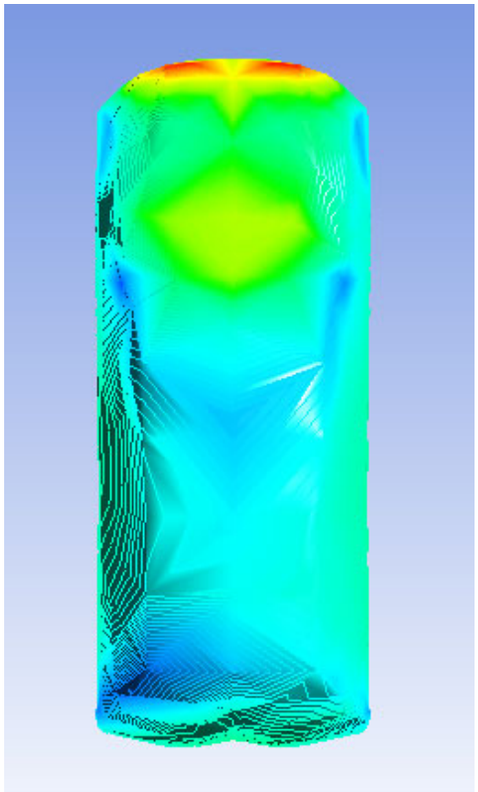

Fig. 7 (a) Pressure distribution of sim. 1.

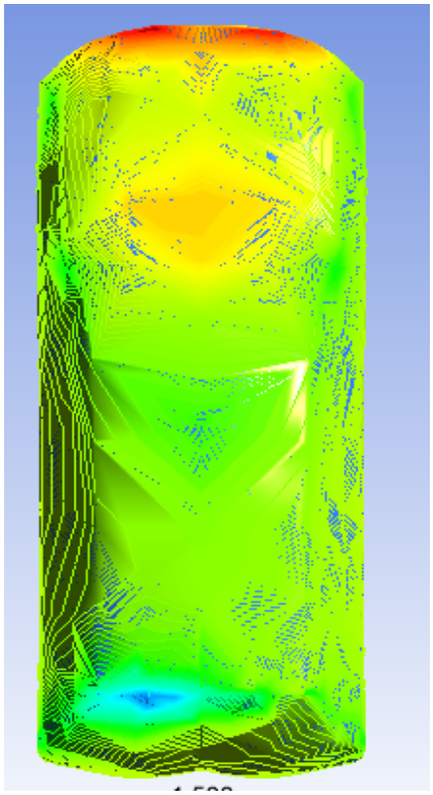

Fig. 7 (b) Pressure distribution of sim. 2.

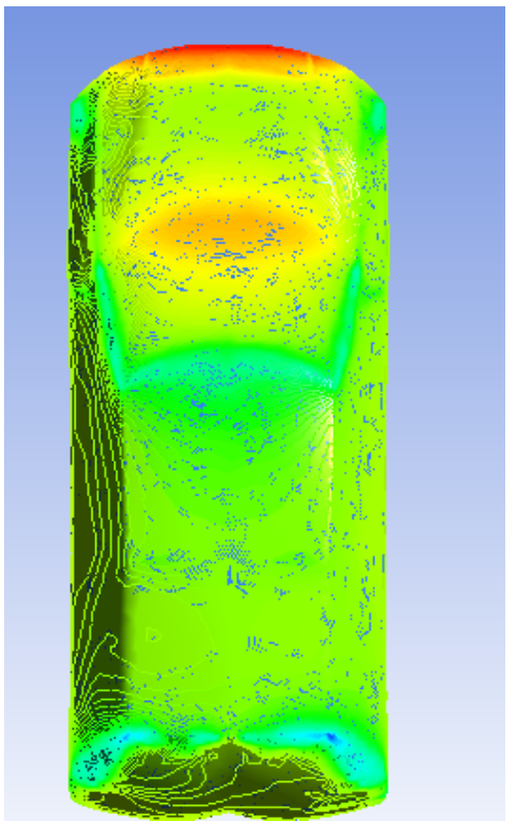

Fig. 7 (c) Pressure distribution of sim. 3

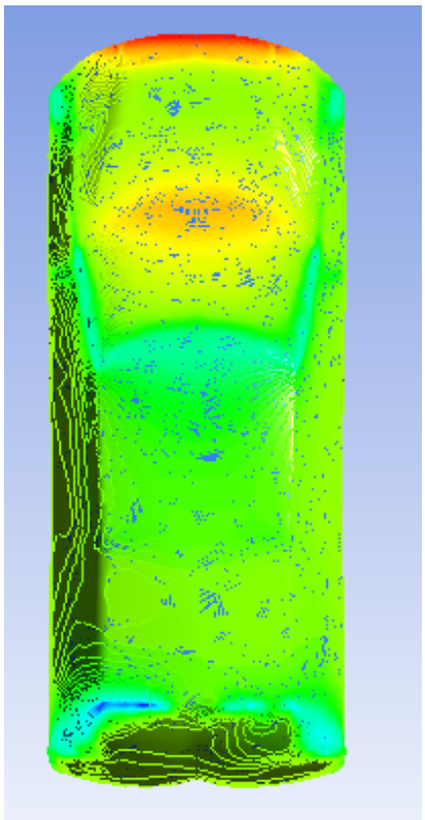

Fig. 7 (d) Pressure distribution of sim. 4

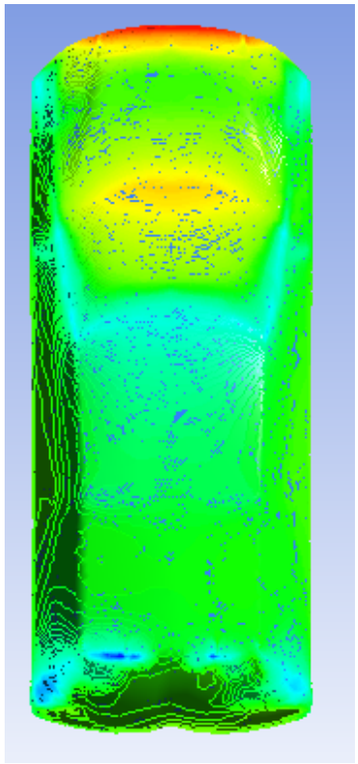

Fig. 7 (e) Pressure distribution of sim. 5

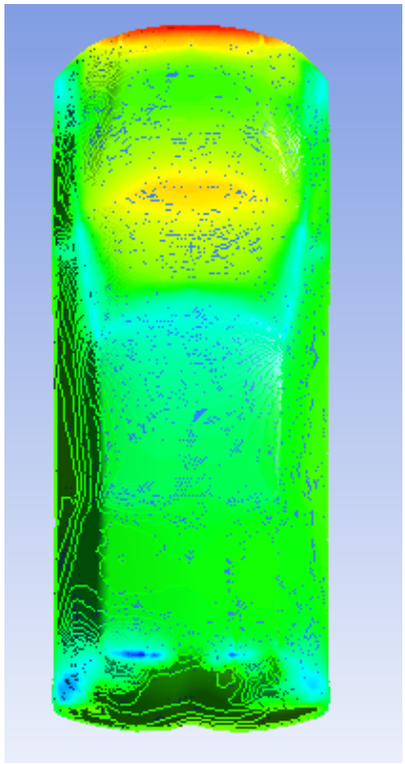

Fig. 7 (f) Pressure distribution of sim. 6

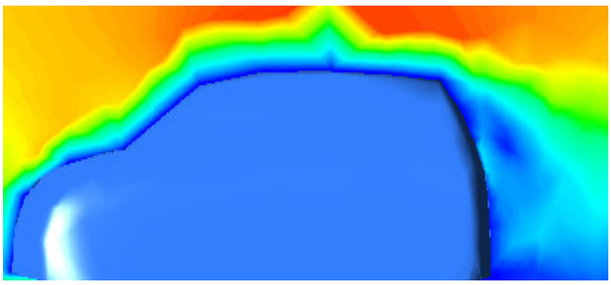

Fig. 8(a) Velocity distribution of sim.1

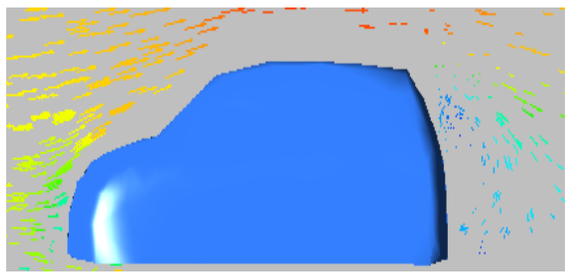

Fig. 8(b) Vel. vectors distribution of sim.1

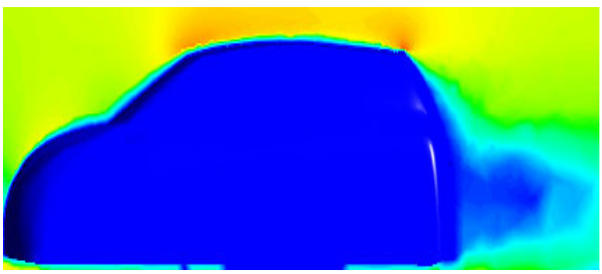

Fig. 8(c) Velocity distribution of sim.2

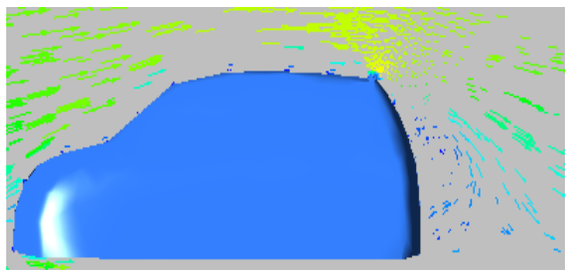

Fig. 8(d) Vel. vectors distribution of sim.2

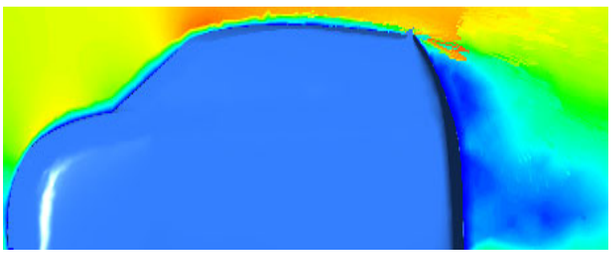

Fig. 8(e) Velocity distribution of sim.3

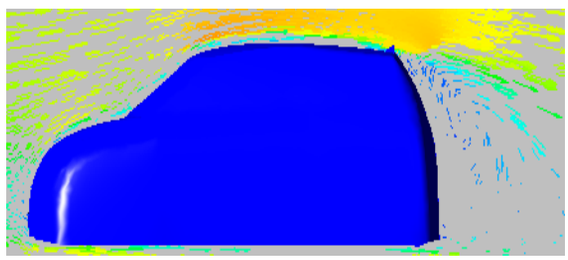

Fig. 8(f) Vel. vectors distribution of sim.3

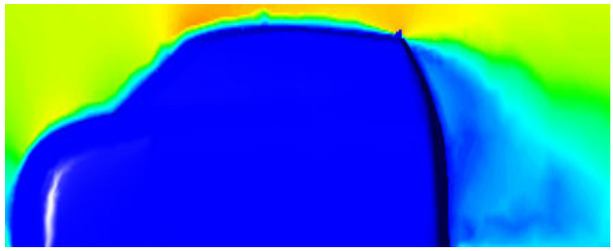

Fig. 8(g) Velocity distribution of sim.4

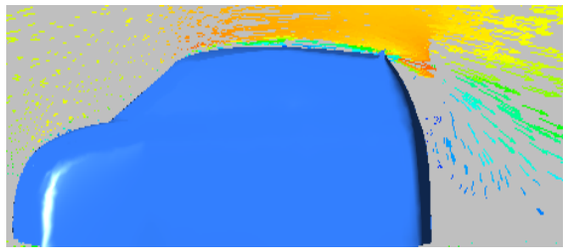

Fig. 8(h) Vel. vectors distribution of sim.4

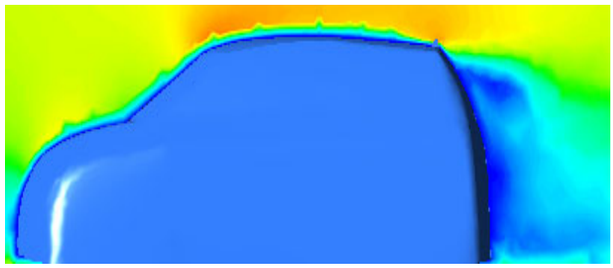

Fig. 8(i) Velocity distribution of sim.5

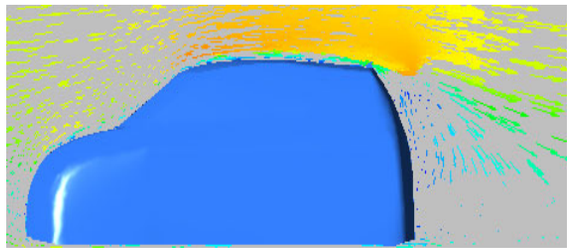

Fig. 8(j) Vel. vectors distribution of sim.5

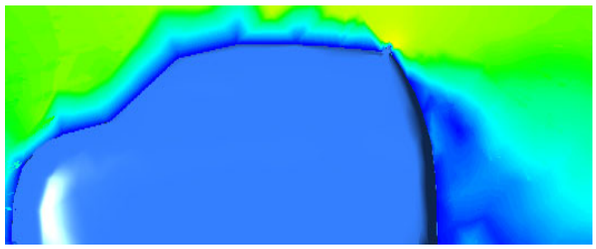

Fig. 8(k) Velocity distribution of sim.6

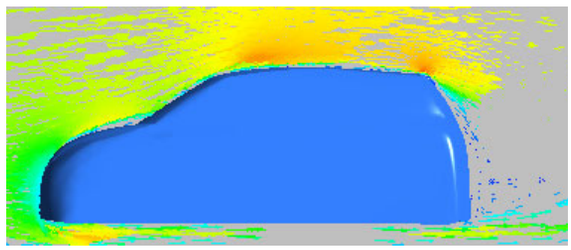

Fig. 8(l) Vel. vectors distribution of sim.6

From the figures, it has been found that there were recirculation zones behind the rear end of the vehicle. This is due to the created low-pressure zone at the rear end, as discussed in 4.1. By comparing the simulation figures, it is seen that the recirculation zone behind the rear end of simulation 1 (without VG, figure 8 (a and b)) is much closer to the rear end of the car compared to other simulations. It indicates the reverse flow of air occurs very near the rear end of the car. This reverse flow ultimately creates drag force. In the simulations 2 and 3 (figures 8 (c) to 8 (f)), as velocity vectors reversed away from the rear end of the car, the drag force decreased. On the other hand, it is seen from the velocity vectors of simulations 4, 5, and 6 (figure 8 (h), (j) and (l)) that at the roof of the car, air flow is also getting reversed, which increases the drag force.

Drag Coefficient

The values of the drag coefficient of all simulations are tabulated in table 3. Figure 9 shows the variation in drag coefficient over the number of VG.

TABLE 3

Drag Coefficient Simulation Results

Simulation Number	Number of VG	Drag Coefficient (C_D)
1	Without VG	0.2468
2	1	0.2183
3	2	0.2210
4	3	0.2319
5	4	0.2440
6	5	0.2442

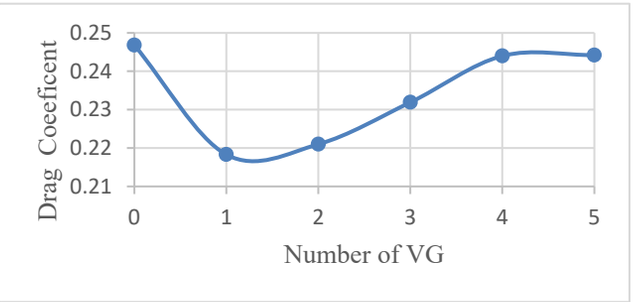

Fig. 9. Number of VG versus drag coefficient.

From table 3 as well as from figure 9, the drag coefficient of a car without VGs is higher compared to a car with 1 or 2 number of VGs. Further, with 4, 5, and 6 number of VGs, the drag coefficient increases. As discussed in sections 4.1 and 4.2, for simulation no. 1, low-pressure zones in the rear-end cause the reverse flow of air in that region and eventually the drag force created in this region.

With the 1 or 2 number VGs on the car, the low-pressure zone gets shifted away from the rear end. Hence, velocity is getting revered away from the rear end. It results in a drag coefficient in these cases being lower than in others.

The 4, 5, or 6 number VGs on the car act as a blunt body in a flow of air. That creates a low-pressure zone at the roof of the car, which results in bad aerodynamics and increases the pressure drag coefficient.

Conclusion

Numerical simulations have been performed on the hatchback car model without and with an increasing number of VGs. Its effects on pressure distribution, velocity distribution, and drag coefficient are investigated in this work. The low-pressure zone behind the moving vehicle is responsible for aerodynamic drag. A VGs were installed to control the low-pressure zone. It was found that without VG, a low-velocity zone is created near the rear end of the car, which causes a high drag force on the car.

The low-velocity zone is shifted away from the rear end of the car when VGs are used, resulting in a decreased drag coefficient. In this study, utilising 1 and 2 numbers of VGs lowered the drag coefficient by up to 11% as compared to without VG.

This study also gives insight on the effects of a number of VGs. It was observed that a greater number of VGs were behaving as blunt bodies in airflow in hatchback cars. This has an adversely effect on the pressure distribution on the car roof. As a result, the drag coefficient of five VGs is higher than the drag coefficient of one VG.

References

[1] Mathieu Roumeas , Patrick Gillieron and Azeddine Kourta 'Drag reduction by flow separation control on a car after body' International Journal For Numerical Methods In Fluids, 2009; 60:1222–1240. https://doi.org/10.1002/fld.1930

[2] Zhigang Yang and Bahram Khalighi 'CFD Simulations for Flow Over Pickup Trucks' SAE Technical Paper Series, 2005-01-0547. https://doi.org/10.4271/2005-01-0547

[3] Ram Bansal and R. B. Sharma 'Drag Reduction of Passenger Car Using Add-On Devices' Hindawi Publishing Corporation Journal of Aerodynamics Volume 2014, Article ID 678518. http://dx.doi.org/10.1155/2014/678518.

[4] Md. Rasedul Islam, Md. Amzad Hossain, Mohammad Mashud, Md. Tanvir Ibny Gias 'Drag Reduction of a Car by Using Vortex Generator' International Journal of Scientific & Engineering Research, Volume 4, Issue 7, July-2013 ISSN 2229-5518

[5] S.M. Rakibul Hassan, Toukir Islam, Mohammad Ali, Md. Quamrul Islam 'Numerical Study on Aerodynamic Drag Reduction of Racing Cars' 10th International Conference on Mechanical Engineering, ICME 2013

[6] R. Himeno, K. Fujitani 'Numerical Analysis and Visualization of Flow in Automobile Aerodynamics Development' Journal of Wind Engineering and Industrial Aerodynamics, 46 & 47 (1993) 785-790

[7] Simon Watkins, Gioacchino Vino 'The effect of vehicle spacing on the aerodynamics of a representative car shape' Journal of Wind Engineering and Industrial Aerodynamics' 96 (2008) 1232–1239. https://doi.org/10.1016/j.jweia.2007.06.042

[8] Diogo Barros, Jacques Bor, Bernd R. Noack, Andreas Spohn and Tony, 'Bluff body drag manipulation using pulsed jets and Coanda effect' Ruiz, Journal of Fluid Mech. (2016), vol. 805, pp. 422–459. https://doi.org/10.1017/jfm.2016.508

[9] H. Viswanathan, 'Aerodynamic performance of several passive vortex generator configurations on an Ahmed body subjected to yaw angles' Journal of the Brazilian Society of Mechanical Sciences and Engineering (2021) 43:131. https://doi.org/10.1007/s40430-021-02850-8

[10] Trebsijg van de Wijdeven, Joseph Katz 'Automotive Application of Vortex Generators in Ground Effect' Journal of Fluids Engineering February 2014, Vol. 136. https://doi.org/10.1115/1.4025917

[11] S Y Cheng and S Mansor, 'Rear-roof spoiler effect on the aerodynamic drag performance of a simplified hatchback model', Journal of Physics: Conf. Series 822 (2017) 012008. https://doi.org/10.1088/1742-6596/822/1/012008

[12] N. Ashton, A. West, S. Lardeau, A. Revell, 'Assessment of RANS and DES methods for realistic automotive models' Computers and Fluids 128 (2016) 1–15. https://doi.org/10.1016/j.compfluid.2016.01.008

[13] Abdellah Ait Moussa, Justin Fischer, and Rohan Yadav 'Aerodynamic Drag Reduction for a Generic Truck Using Geometrically Optimized Rear Cabin Bumps' Hindawi Publishing Corporation Journal of Engineering Volume 2015, Article ID 789475. https://doi.org/10.1155/2015/789475

[14] Darko Damjanovic, Drazan kozak, Marija Zivic, Zeljko Ivandic, Tomislav Baskaric 'CFD analysis of concept car in order to improve aerodynamics' Scientific and Expert Conference TEAM 2010, Kecskemet, November 4-5, 2010

[15] M. Rouméas, P. Gilliéron and A. Kourta, 'Drag Reduction by Flow Separation Control on a Car after Body', International Journal for Numerical Methods in Fluids, 60(2009) 1222–1240. https://doi.org/10.1002/fld.1930

[16] Yifei Wang, Christophe Sicot, , Jacques Boree, Mathieu Grandemange, 'Experimental study of wheel-vehicle aerodynamic interactions', Journal of Wind Engineering and Industrial Aerodynamics Volume 198, March 2020, 104062

[17] Mark Pastoor Lars Henning Bernd R. Noack, Rudibert King ,Gilead Tadmor, 'Feedback shear layer control for bluff body drag reduction', Journal of Fluid Mechanics , Volume 608 , 10 August 2008 , pp. 161 – 196. https://doi.org/10.1017/S0022112008002073

[18] Cheng, S.Y., Tsubokura, M., Nakashima, T., Nouzawa, T., Okada, Y., 'A numerical analysis of transient flow past road vehicles subjected to pitching oscillation', Journal of Wind Engineering and Industrial Aerodynamics Volume 99, Issue 5, May 2011, Pages 511-522. https://doi.org/10.1016/j.jweia.2011.02.001

[19] Charles-Henri Bruneaua ,Emmanuel Creuséb, Patrick Gilliéronc, Iraj Mortazavia, 'Effect of the vortex dynamics on the drag coefficient of a square back Ahmed body: Application to the flow control', European Journal of Mechanics - B/Fluids Volume 45, May–June 2014, Pages 1-11. http://dx.doi.org/10.1016/j.euromechflu.2013.11.003

[20] L.Salati, P.Schito, F.Cheli, 'Strategies to reduce the risk of side wind induced accident on heavy truck', Journal of Fluids and Structures Volume 8 8, July 2019, Pages 331-351. https://doi.org/10.1016/j.jfluidstructs.2019.05.004

[21] Sang Wook Lee, Hak Lim Kim, 'Numerical Study of Active Aerodynamic Control via Flow Discharge on a High-Camber

Rear Spoiler of a Road Vehicle' Applied Science, 2019, 9(22), 4783.
https://doi.org/10.3390/app9224783

[22] Alamaan Altaf, Ashraf A. Omar , Waqar Asrar, 'Passive drag reduction of square back road vehicles', Journal of Wind Engineering and Industrial Aerodynamics Volume 134, November 2014, Pages 30-43.
http://dx.doi.org/10.1016%2Fj.jweia.2014.08.006

[23] Xin-kai Li, Wei Liu Ting-jun, Zhang, Pei-ming Wang and Xiao-dong Wang, 'Analysis of the Effect of Vortex Generator Spacing on Boundary Layer Flow Separation Control', Applied Science Journal . 2019, 9, 5495.
https://doi.org/10.3390/app9245495

[24] Xin-Kai Li ,Wei Liu 1,Ting-Jun Zhang, Pei-Ming Wang and Xiao-Dong Wang, 'Experimental and Numerical Analysis of the Effect of Vortex Generator Installation Angle on Flow Separation Control' Energies 2019, 12(23), 4583.
https://doi.org/10.3390/en12234583

Address correspondence to: *Mr. Sanjay D. Patil, Assistant Professor, Department of Automobile Engineering, Government College of Engineering and Research, Avasari, Pune - Maharashtra.*
Ph: 09029719392
Email: sanjaypatil365@gmail.com; sdpatil.auto@gcoeara.ac.in